

# Dynamic properties and liquefaction behaviour of granular materials using discrete element method

S. V. Dinesh<sup>1,\*</sup>, T. G. Sitharam<sup>2</sup> and J. S. Vinod<sup>2</sup>

<sup>1</sup>Department of Civil Engineering, Siddaganga Institute of Technology, Tumkur 572 103, India

<sup>2</sup>Department of Civil Engineering, Indian Institute of Science, Bangalore 560 012, India

**Dynamic properties of the soil such as shear modulus and damping ratio are important parameters in the prediction of the dynamic response of geotechnical engineering structures. Though these properties are dependent on several factors, strain amplitude and confining pressure have a major effect. Liquefaction is another important phenomenon associated with the undrained response of granular materials in loose state. In this paper, the results of the numerical simulation of cyclic triaxial shear tests on three-dimensional assembly consisting of 1000 sphere particles using Discrete Element Method (DEM) have been reported under undrained conditions. From the results, the shear modulus and damping ratio have been estimated for a range of shear strain and confining pressure. The DEM simulations have modeled the liquefaction behaviour under undrained conditions very close to the real experimental behaviour.**

THE dynamic response of ground and soil structures is dependent on the shear modulus ( $G$ ) and damping ratio ( $D$ ). These properties are dependent on soil type, gradation characteristics, number of cycles of dynamic load application, magnitude of shear strain and confining pressure. Among the above factors the magnitude of shear strain and the confining pressure have greater effect on the shear modulus and damping ratio. At low shear strain levels (around  $10^{-6}$ ) the soil will behave as an elastic material with low damping value. With increase in shear strain amplitude, soil shows plastic behaviour with a greater degree of non-linearity resulting in decrease in shear modulus and an increase in damping. This kind of characterization of the behaviour is more difficult. The advanced cyclic nonlinear models coupled with pore-pressure that are used to predict the changes in effective stress due to changes in cyclic loading require the modulus degradation curves. Therefore low and large shear strain levels certainly influence the dynamic strength and deformation characteristics. Low strain level dynamic properties are measured from Resonant column test, Ultrasonic pulse test, Piezoelectric bender element test. Large strain level dynamic properties are mea-

sured from cyclic triaxial test, cyclic direct shear test, cyclic torsional shear test. Also during repeated application of a shear stress under undrained conditions, the sandy soil may lose the shear strength under monotonic and cyclic loading. This occurs because the excess pore water pressure does not return to zero after each unloading, but rather accumulates. With sandy soils, this behaviour during cyclic loading may cause nearly total loss of resistance to shear, and soil may reach the liquefied state. The cumulative build-up of pore water pressure causes the effective stress path to move towards the origin. When the effective stress reduces to zero value, the soil is said to be in initial liquefied state<sup>1</sup>. This type of liquefaction failure is characteristic of low density saturated granular materials under undrained conditions. If the material is dense then the particles cannot move into the void spaces and would move up against the adjacent soil grains causing dilation and there will be an increase in effective stress and decrease in pore water pressure. The cyclic behaviour is generally obtained from analytical models based on continuum approach and by appropriate cyclic triaxial tests in the laboratory. Analytical models assume continuum behaviour though the soil is multiphase particulate medium. The continuum models are phenomenological and do not consider the particulate behaviour of granular materials and this certainly affects the deformation and failure modes. The triaxial test on cylindrical soil specimens is the most commonly performed test to study the cyclic behaviour of sands. However, triaxial testing has limitations, especially with sands like non uniformity of strains and stress fields, end restraint effects, membrane penetration effects and difficulties in preparing identical loose specimens at low confining pressures. Also the response depends on the methods of sample preparation and rate of testing, etc. Hence quantitative evaluation of several aspects of soil behaviour by experimentation still remains quite problematic.

The danger caused by liquefaction during earthquake has necessitated the need to investigate the mechanism of loss of shear strength. Many researchers are of the opinion that the liquefaction is due to pore pressure development, which results in reduction in effective stress. Though the earlier studies regarding the dynamic properties and liquefaction have added to the understanding of the mechanism

\*For correspondence. (e-mail: s\_v\_dinesh@hotmail.com)

it was felt necessary to understand this from a more fundamental way considering the particulate nature of the granular materials. In this investigation, the granular media has been considered as an assemblage of particles rather than as a continuum. Discrete Element Method (DEM) pioneered by Cundall<sup>2</sup>, in which the elements or grains can freely make and break contacts with their neighbours very similar to the particulate behaviour, has been used.

A comprehensive numerical simulation program of cyclic triaxial shear tests under undrained (constant volume – no pore-water pressure has been included in the analysis) conditions is performed on an assemblage consisting of 1000 polydisperse spheres. The dynamic properties and the macroscopic cyclic test results are presented. Parameters such as shear modulus, damping, strain amplitudes, confining pressure and number of cycles required for liquefaction have been considered.

### Discrete element method

The Discrete Element Method was pioneered by Cundall<sup>2,3</sup> to model the analysis of rock slopes and also to develop a model for two-dimensional assemblies of circular discs<sup>4,5</sup>. They have developed a FORTRAN code BALL implementing DEM and used to model the granular materials based on micromechanical considerations. Modified versions of BALL was used by various researchers<sup>6-15</sup> extensively for understanding the constitutive behaviour of granular materials. In 2D, there is problem in comparing the results with the experimental behaviour. This difficulty was overcome by the development of the program TRUBAL<sup>16,17</sup> that models three-dimensional assemblies. The modified versions of TRUBAL have been used extensively to study the constitutive behaviour of granular assemblies<sup>18-26</sup>. The fundamental idea of DEM is that each particle is modeled as an element obeying Newton's second law of motion. Equilibrium contact forces and displacements are found in a stressed assembly of particles through a series of calculations tracing the movement of each particle. The movement of each particle is tracked by solving a set of Newton's equations of motion. A contact force generates when the elements overlap and the magnitude of contact force is determined by the force-displacement law. Coulomb's friction law is adopted for the relative slippage between elements. A suitable damping in the form of Rayleigh damping is incorporated to dissipate the kinetic energy generated. The resultant force vector on each element is the vectorial sum of contact forces. The law of motion is applied to each sphere during the time step. The particle accelerations, velocities and displacements are obtained by integrating the law of motion and are assumed to be constant over a time step. During the next time step, new set of contact forces on a sphere particle is obtained from force-displacement law and the cycle of calculation will continue. Force boundary conditions, displacement

boundary conditions and gravitational loads can be applied on the system. In DEM, internal stresses and contact behaviour can be captured efficiently, and sample reproducibility is guaranteed. The major advantage is the wealth of micromechanical and statistical information that can be generated by the DEM simulations along with the macroscopic response.

To simulate 3-dimensional assembly of sphere particles the version TRUBAL, Chantawarungal<sup>19</sup> of the University of Waterloo, Canada, modified and updated at the Indian Institute of Science has been used for the simulations.

### Numerical simulation details

The numerical scheme employs the periodic space where the opposite faces are numerically connected. Therefore the assembly is free from boundary constraints and any assembly with finite number of particles constitutes an infinite system.

Each sphere has prescribed properties including a radius, density, and coefficient of contact friction. The input parameters used in the simulations are as shown in Table 1.

#### Assembly generation

Three-dimensional assembly consisting of 1000 sphere particles having diameters ranging from 0.40 to 2.00 mm consisting of 21 different sizes corresponding to log normal distribution are generated in a periodic space by a random number generator according to desired particle size in a random manner. These particles are mapped in to the specified area. Particles with largest diameter are generated first and the smallest last. Figure 1 shows the initially generated assembly without any initial contacts.

#### Sample compaction and testing

The objective of this work is to estimate the shear modulus and damping ratio over a range of shear strain and confining pressure to evaluate dynamic properties and to understand the liquefaction behaviour of granular materials under undrained cyclic loading conditions particularly at low confining pressures. In order to obtain a loose assembly that liquefies on shearing, a friction coefficient of 0.5 is assigned.

**Table 1.** Input parameters selected for the numerical simulations

Properties	Symbols	Numerical values used
Normal contact stiffness	$K_n$	$1.0 \times 10^5$ N/m
Tangential contact stiffness	$K_t$	$1.0 \times 10^5$ N/m
Particle density	$\rho$	2000 kg/m <sup>3</sup>
Cohesion	$C$	0.0
Contact friction	$\mu$	0.5

ned to all particle contacts. Then the cubic space is compressed isotropically by distorting the periodic cell and changing its volume under strain controlled loading condition initially. Later the assembly is compressed under  $s_{11} = s_{22} = s_{33}$  condition using a servo control as  $\dot{\mathbf{e}}_{kk} = \dot{\mathbf{e}}_{kk} + \frac{g}{3}(\mathbf{s}_{kk}^{\text{specified}} - \mathbf{s}_{kk}^{\text{measured}})$  to the required level of compression where  $g$  is the specified servo gain. To ensure a stable system at the specified stress state the calculation cycles were continued, till the void ratio, average coordination number and stress values are constant. At the desired stress state the assembly configurations are saved for cyclic triaxial tests. Figure 2 shows the isotropically compacted loose stable assembly at a confining pressure of 25 kPa.

A comprehensive numerical simulation program is carried out to evaluate the dynamic properties and to understand the liquefaction behaviour of granular materials. Constant strain amplitude cyclic triaxial tests under undrained conditions are carried out on samples at different confining pressures at different shear strain amplitudes. Table 2 shows the details of numerical simulations carried out.

**Results and discussions**

For triaxial stress state, the elastic modulus ( $E$ ) and the shear modulus ( $G$ ) are obtained from

$$E = \frac{\mathbf{s}_d}{\mathbf{e}}, \tag{1}$$

$$\mathbf{g} = (1 + \mathbf{m})\mathbf{e}, \tag{2}$$

$$G = \frac{E}{2(1 + \mathbf{m})}, \tag{3}$$

where  $\mathbf{s}_d$  = Deviator stress,  $\mathbf{g}$  = Shear strain,  $\mathbf{e}$  = Axial strain and  $\mathbf{m}$  = Poisson's ratio.

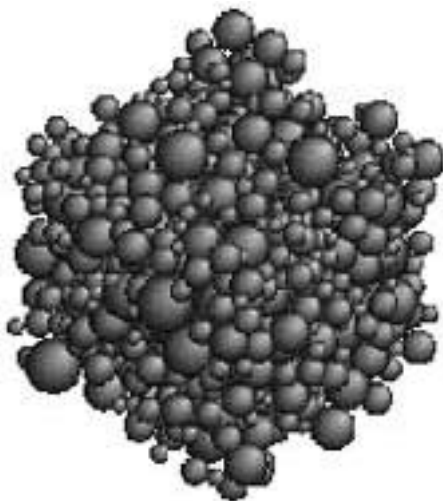


**Figure 1.** 3-D view of the initially generated assembly without overlaps.

The damping ratio ( $D$ ) is measured from the hysteresis loop as shown in Figure 3 (ref. 27).

$$D = \frac{A_L}{4pA_T} \tag{4}$$

where  $A_L$  = Area enclosed by the hysteresis loop,  $A_T$  = Area enclosed by the shaded triangle.

The macroscopic results are described in terms of effective mean normal stress, ( $p$ ) and deviator stress ( $q$ ), which are defined as follows

$$p = \frac{\mathbf{s}'_{11} + \mathbf{s}'_{22} + \mathbf{s}'_{33}}{3}; q = \sqrt{\frac{3}{2}\mathbf{s}'_{ij}\mathbf{s}'_{ij}}, \tag{5}$$

where  $\mathbf{s}'_{ij}$  is the deviatoric stress tensor.

For the triaxial tests in the present study with symmetry in directions 2 and 3 ( $\mathbf{s}'_{22} = \mathbf{s}'_{33}$ ) the stress parameters are

$$p = \frac{\mathbf{s}'_{11} + 2\mathbf{s}'_{33}}{3}; q = \mathbf{s}_{11} - \mathbf{s}_{33}. \tag{6}$$

*Shear modulus.* Figure 4 shows the relationship between the shear modulus and the shear strain for confining pressures of 25, 50 and 100 kPa. The same shear modulus is normalized by  $G_{\text{max}}$  (usually taken to be the modulus at a shear strain  $10^{-4}\%$ ) for the same range of confining pressure. Figure 5 shows the normalized plot  $G/G_{\text{max}}$  versus shear strain for different confining pressures. It is observed from Figures 4 and 5 that with increase in shear strain there is a reduction in the shear modulus and  $G/G_{\text{max}}$  value. The reduction is significant beyond a shear strain of 0.01 indicative of the transition from elastic to plastic behaviour. It is apparent from the figure that the curve shifts consistently to the right as confining pressure increases, which is in very good agreement with experimental results of sands<sup>28</sup>.

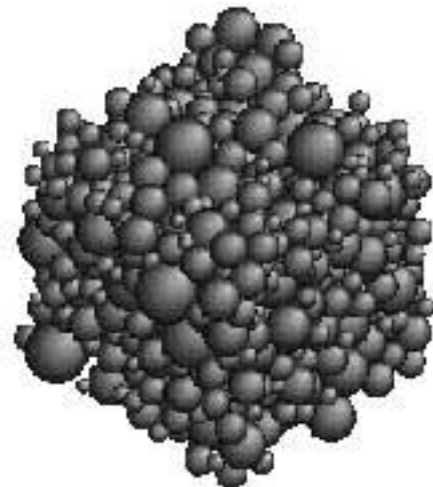


**Figure 2.** 3-D view of the compacted assembly.

**Table 2.** Programme of numerical simulations of cyclic triaxial shear tests

Test no.	Test path during shear test	Boundary control (strain rate)	Void ratio	Confining pressure (kPa)	Remarks
1	Undrained	1%	0.6	5	Effect of strain amplitude/ confining pressure
2	Undrained	1%	0.59	10	
3	Undrained	1%	0.57	15	
4	Undrained	1%	0.56	20	
5	Undrained and drained	0.01, 0.1, 0.15 0.25, 0.5, 1, 2, 3% and 1.4, 2 and 3%	0.55	25	
6	Undrained	0.01, 0.1, 0.15 0.25, 0.5 and 1%	0.5	50	
7	Undrained	0.01, 0.1, 0.15 0.25, 0.5 and 1%	0.42	100	

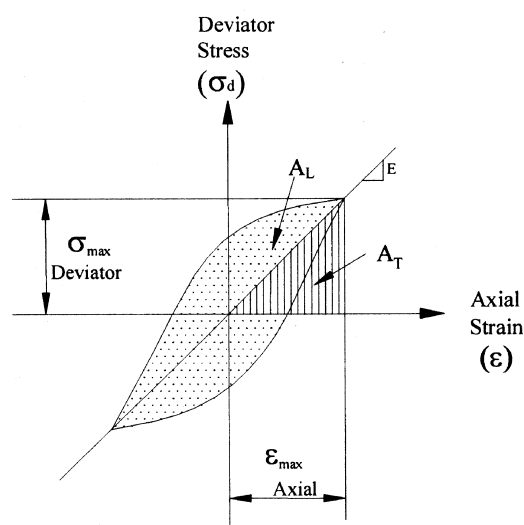


**Figure 3.** Hysteretic stress–strain relationship.

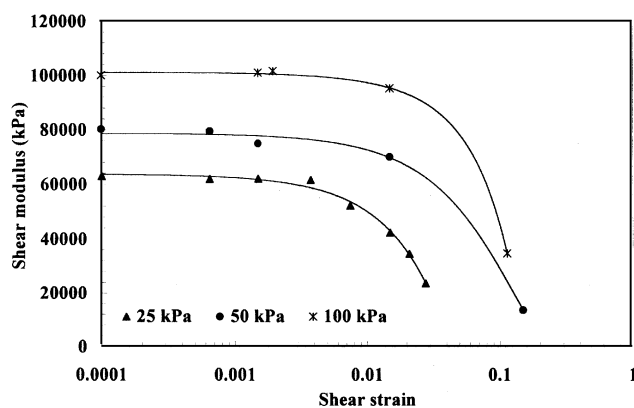


**Figure 4.** Shear modulus versus shear strain.

**Damping.** Figure 6 shows the plot of damping ratio ( $D$ ) versus shear strain for 25, 50 and 100 kPa confining pressure. It is observed that at any given shear strain level samples under low confining pressures have greater damping. It is clearly observed that there is an increase in damping

with increase in shear strain very similar to the experimental observation. Also at any strain level, damping increases with reduction in confining pressure. The results are in good agreement with experimental results found on sands<sup>28</sup>.

This shows that the DEM simulations have captured the shear modulus and damping variation trend very similar to the experimental results of Kokusho<sup>28</sup> and Yasuda and Matsumoto<sup>29</sup>.

**Liquefaction.** Figure 7 shows the results of undrained cyclic test at 1% deviatoric strain amplitude on a sample at a confining pressure of 25 kPa corresponding to a void ratio of 0.55.

Figure 7a shows the plot of deviator stress ( $q$ ) vs mean principal stress  $p$ . In this test with loading and unloading cycles, there is a gradual and steady decrease in mean normal stress ( $p$ ) and deviator stress ( $q$ ). The magnitude of deviator stress on compression side is higher than on extension side. Pore water pressure progressively builds up, causing effective stress path to migrate towards the origin. It requires 34 cycles for the sample to undergo complete liquefaction.

Figure 7b shows the plot of deviatoric stress ( $q$ ) vs deviatoric strain ( $\epsilon_s$ ) at 1% deviatoric strain amplitude. The sample attains a peak deviator stress of 12.7 kPa in the first cycle (46% of peak static strength). Thereafter deviator stress reduces gradually in successive cycles and finally reaches zero deviator stress level, thereby undergoing complete liquefaction. This indicates liquefaction at deviator stress smaller than the static strength also at smaller deviator strain levels.

Figure 7c shows the plot of average co-ordination number (number of contacts per particle) vs mean principle stress ( $p$ ). The average co-ordination number also decreases steadily during the test due to cyclic loading from a value of 4.25 to 2.75 after which sample becomes unstable and collapses undergoing complete liquefaction. The decrease in average coordination number will be reflected as a decrease in mean principal stress ( $p$ ) or increase in pore-water pressure.

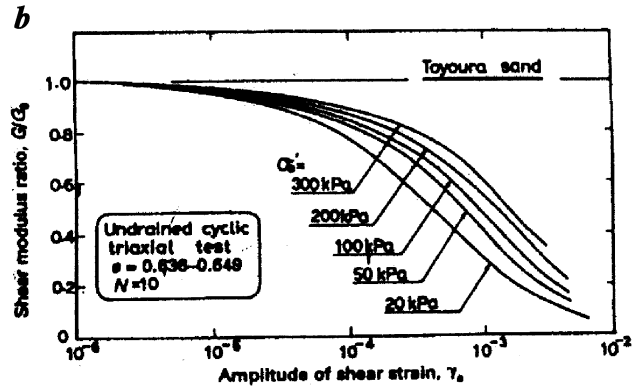
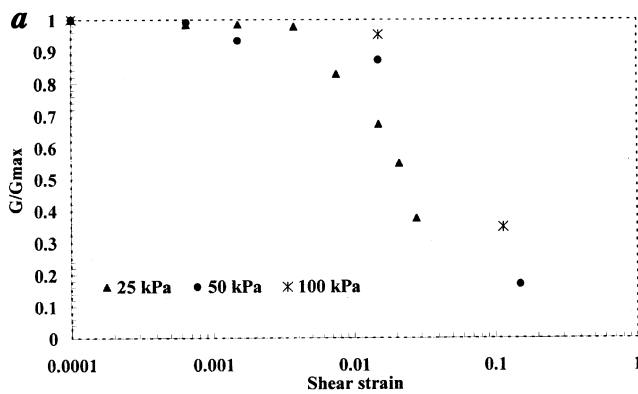


Figure 5. *a*, Normalized shear modulus versus shear strain for different confining pressures; *b*, Normalized shear modulus versus amplitude of shear strain<sup>28</sup>.

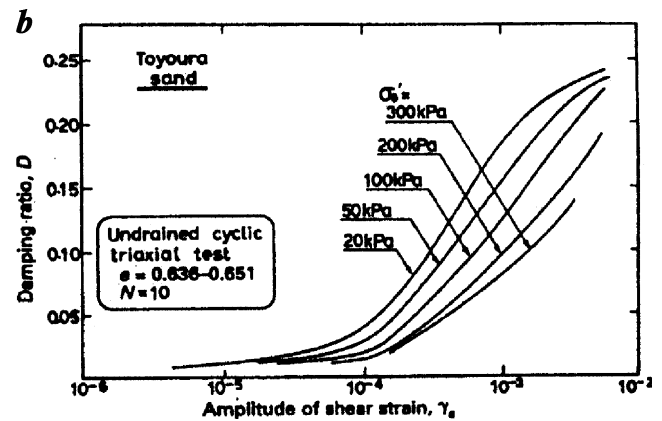
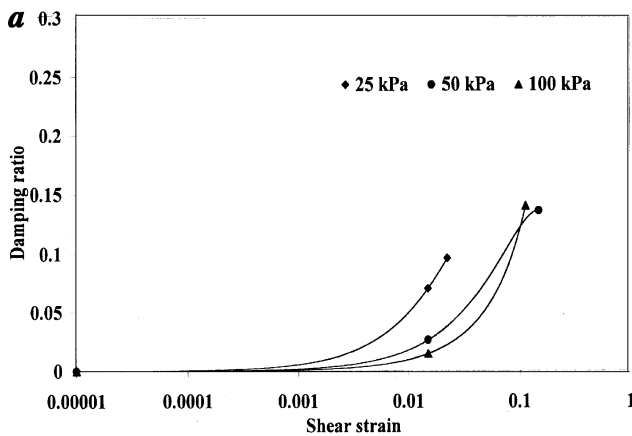


Figure 6. *a*, Damping ratio versus shear strain; *b*, Damping ratio versus amplitude of shear strain<sup>28</sup>.

Figure 7d shows the plot of average coordination number versus deviator stress ( $q$ ). Under successive cycles with reduction in deviator stress the average coordination number also reduces gradually in an irreversible way. There is a decrease in the average coordination number during both compression and extension loading phases. The assembly shows instability from the beginning. Upon reversal in the direction of shear strain there will be contact disintegration between the neighbouring particles, which results in pore water pressure increase. There is a gradual decrease in deviator stress with reduction in average coordination number till the average coordination number is around 3. When the average coordination number is around 3 or less the assembly cannot withstand even the low stresses prevailing at that stage and it buckles resulting in collapse.

Undrained cyclic triaxial shear tests at 1.4, 2 and 3% deviatoric strain amplitudes have also indicated similar behaviour.

Figure 8 shows the plot of cyclic stress ratio [ratio of applied deviator stress in the first cycle on the compression side to confining pressure] (CSR) versus number of cycles for liquefaction at 1%, 1.4%, 2% and 3% deviator

strain amplitude. It is clearly observed that with increase in strain amplitude the applied deviator stress will be more, as a result there is an increase in the cyclic stress ratio and reduction in number of cycles for liquefaction state. Up to 2% deviatoric strain level the relationship is linear and beyond this the increase in CSR is nonlinear. Under high cyclic stress ratio the sample undergoes liquefaction in lesser number of cycles, indicative of higher liquefaction potential.

Figure 9 shows the results of drained cyclic test on loose sample at 25 kPa confining pressure at 1.3% deviator strain amplitude. The results show that the peak deviator stress on compression side is (15–17.9 kPa) more than on extension side (13.8–15 kPa). There is an increase in stress ratio with cycles and the increase is more on compression (0.6–0.72) side than on extension (0.55–0.6) side. There is no significant variation in the value of average co-ordination number. It oscillates within a narrow range upon reversal of loading directions. Clearly a gain of contacts is observed on compression and loss of contacts on extension side. The magnitude of gain and loss of contacts is nearly same in a cycle. The deviatoric strength and mean principle stress are

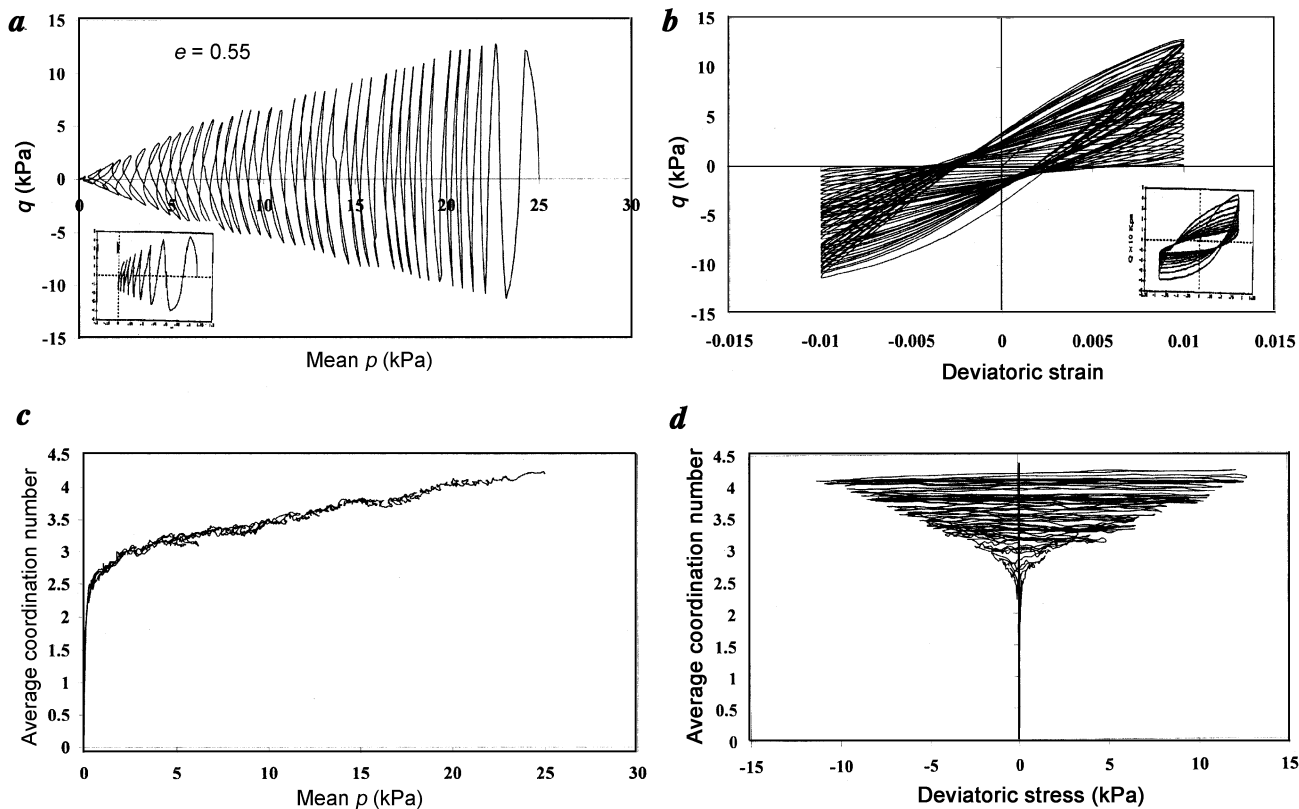


**Figure 7.** Results of undrained cyclic test on loose sample at 1% deviatoric strain amplitude. *a*, Deviator stress  $q$  versus mean  $p$ ; *Inset*, Deviatoric stress versus number of cycles<sup>30</sup>; *b*, Deviator stress versus deviatoric strain; *Inset*, Deviator stress versus deviatoric strain<sup>30</sup>; *c*, Average coordination number versus mean  $p$  and *d*, Average coordination number versus deviatoric stress.

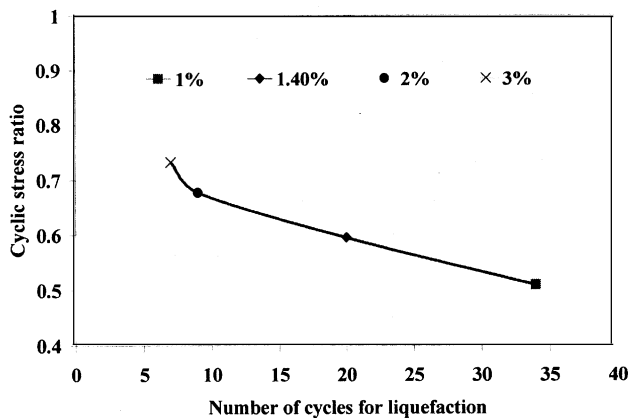


**Figure 8.** Plot of cyclic stress ratio vs number of cycles for liquefaction.

constant as the test progresses. The sample shows compressive volumetric strain. The magnitude of volumetric strain (0.00462) is more in the first cycle and it reduces in the subsequent cycles. The compressive volumetric strain is more and more plastic in the initial cycles and irrecoverable. With compression it develops (gains) contacts that are lost during unloading to maintain equilibrium and there will be no reduction in deviator stress and mean

principle stress. Different parameters will be operating within certain range. The assembly does not show any signs of liquefaction. The results of drained cyclic test at 2 and 3% deviatoric strain amplitude indicate similar behaviour with no liquefaction tendency but the sample undergoes large volumetric strains.

It can be concluded that granular materials undergo liquefaction under undrained conditions and the magnitude of deviatoric strain amplitude affects liquefaction. Higher the magnitude of deviatoric strain amplitude, greater is the liquefaction potential. Samples liquefy even under low magnitudes of deviator stress levels compared to the static strength. Small amplitudes of deviatoric strain also cause liquefaction. In a drained test granular materials never liquefy. This is because there will be volumetric compression with gain of contacts and during unloading, dilation of particles occur with a small number of loss of contacts. Even during dilation the sample undergoes a net volumetric compression. The results of numerical simulations during undrained and drained conditions on 3-dimensional sphere assemblies qualitatively compare well with the cyclic triaxial test results reported<sup>30,31</sup>.

Figure 10 shows the results of undrained cyclic tests at confining pressures of 5, 10, 15, 20, 25 and 50 kPa respectively. The results show that the deviator stress and

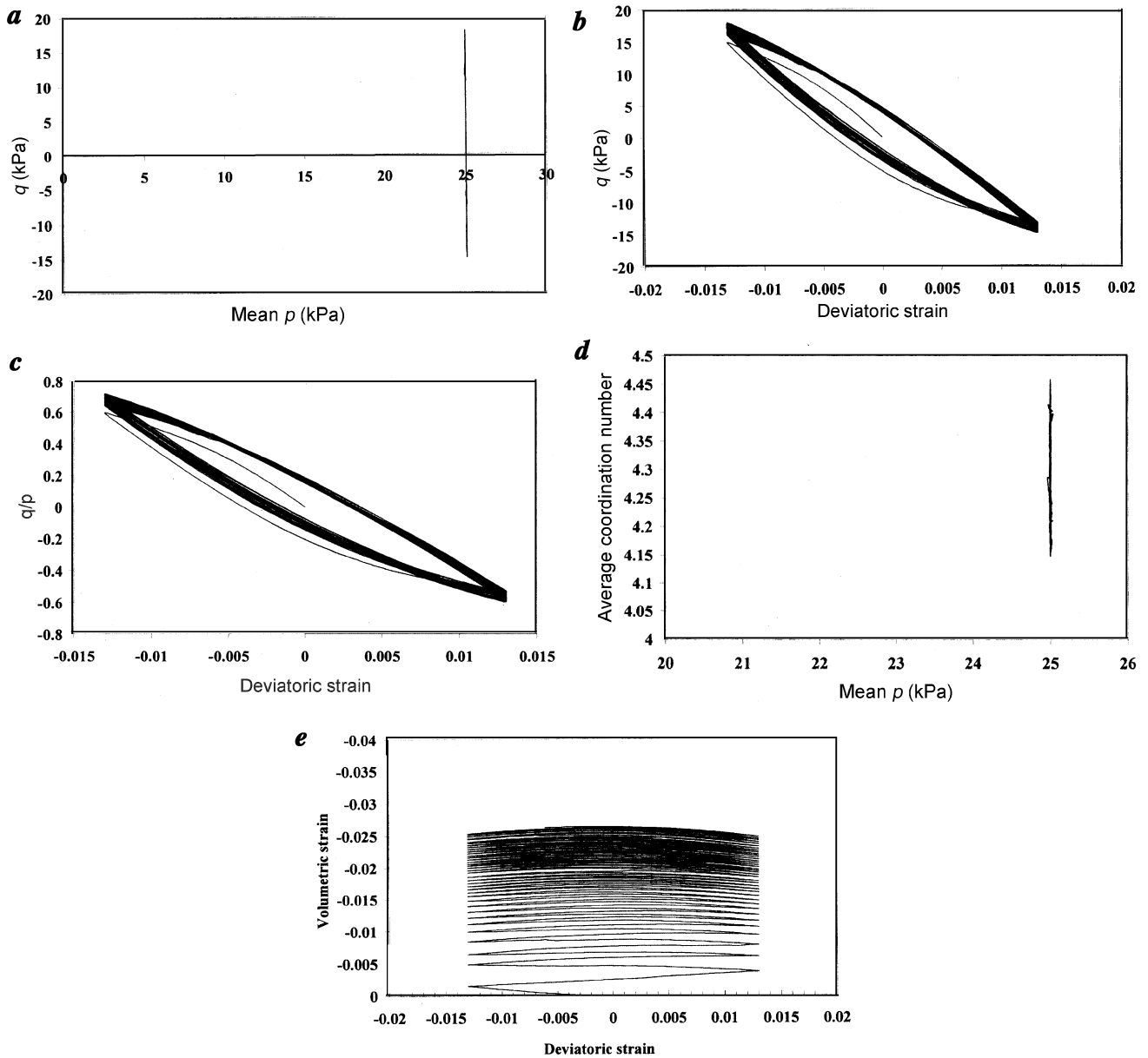


**Figure 9.** Results of drained cyclic test at 25 kPa confining pressure. *a*, Deviator stress versus mean  $p$ ; *b*, Deviator stress versus deviatoric strain; *c*, Stress ratio ( $q/p$ ) versus deviatoric strain; *d*, Average coordination number versus mean  $p$ ; *e*, Volumetric strain versus deviatoric strain.

mean principal stress  $p$  reach zero and the assemblies liquefy at 1, 3, 8, 20 and 34 cycles at 5, 10, 15, 20 and 25 kPa respectively indicating that with increase in confining pressure there is an increase in the liquefaction resistance. All samples fail during loading from extension to compression side. A higher deviator stress on compression side than extension side is observed at all confining pressures. But at 50 kPa confining pressure the results show that the deviator stress attains a fairly constant value (20 kPa) on the compression and extension side (18 kPa). There is a large reduction in mean principal stress during the first cycle and thereafter reduction in mean principle stress is only marginal. Mean principal stress ( $p$ ) reduces marginally by

about 9% from its initial value beyond which there is no reduction. There is no liquefaction of the sample.

This is indicative of the fact that with increase in confining pressure there is an increase in liquefaction resistance but it requires several fold increase in confining pressure to eliminate the risk of liquefaction.

Figure 11 shows the plot of number of cycles for complete liquefaction for the above tests at different confining pressures. It is observed that at low confining pressures, i.e. at less than 10 kPa the assembly liquefies at smaller number of cycles, beyond 10 kPa and up to 25 kPa there is linear increase in the number of cycles required for liquefaction with increase in confining pressure.

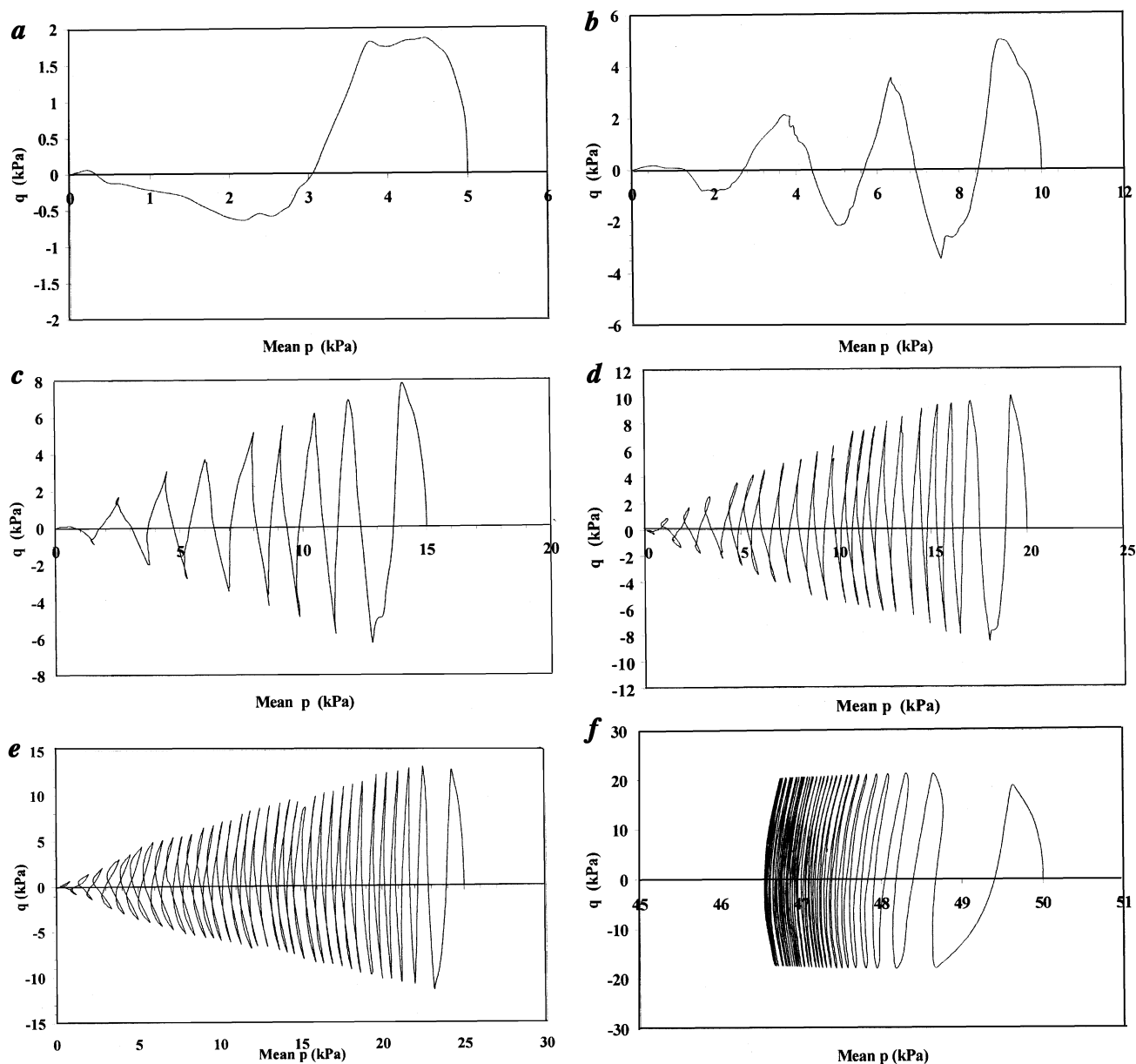


Figure 10. Deviator stress versus mean principal stress at (a) 5 kPa; (b) 10 kPa; (c) 15 kPa; (d) 20 kPa; (e) 25 kPa; (f) 50 kPa.

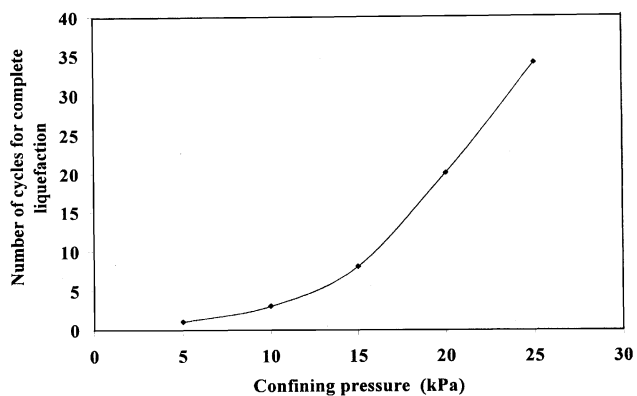


Figure 11. Plot of number of cycles for complete liquefaction vs confining pressure at 1% deviator strain level.

### Conclusions

The discrete element simulation results presented in this paper have captured the dynamic properties and the liquefaction behaviour of granular materials very similar to the experimental results reported<sup>28-31</sup>. These numerical simulations offer a unique opportunity to obtain complete qualitative information, thus making it possible to look at the physical processes that govern the cyclic behaviour. There is a reduction in shear modulus and an increase in damping at large shear strain levels. Loose samples liquefy under cyclic loading under undrained conditions at much smaller deviator stress levels than their static strength. Liquefaction is due to continued cumulative loss of aver-

age coordination number under each reversal of loading due to continuous reorientation of fabric. Assemblies under initial loose conditions liquefy rapidly with increase in strain amplitude. At low confining pressure assembly liquefies rapidly but with increase in confining pressure there is an increase in liquefaction resistance but it requires a several-fold increase of confining pressure to eliminate the risk of liquefaction.

1. Seed, H. B. and Lee, K. L., Liquefaction of saturated sands during cyclic loading. *J. Soil Mech. Found Div., ASCE*, 1966, **92**, 105–134.
2. Cundall, P. A., A computer model for simulating progressive, large-scale movements in blocky rock systems. Proceedings of the Symposium Soc. Rock Mechanics, 1971, p. 12.
3. Cundall, P. A., Explicit finite difference methods in geomechanics. Proceedings of the 2nd International Conference on Numerical Methods in Geomechanics, Blacksburg, Virginia, 1976, pp. 132–150.
4. Strack, O. D. L. and Cundall, P. A., The discrete element method as a tool for research in granular media. I, Report to National Science Foundation, Department of Civil and Mineral Engineering, University of Minnesota, Minneapolis, Minnesota, 1978, p. 97.
5. Cundall, P. A., BALL – A Computer Program to Model Granular Media Using the Distinct Element Method. Technical Note TN-LN-13, Advance Technology Group, Dames and Moore, London, 1978, pp. 129–163.
6. Bathurst, R. J., A study of stress and anisotropy in idealized granular assemblies, PhD dissertation, Queen's University, Kingston, Canada, 1985.
7. Bathurst, R. J. and Rothenburg, L., Micromechanical aspects of isotropic granular assemblies with linear contact interactions. *J. Appl. Mech., ASME*, 1988, **55**, 17–23.
8. Bathurst, R. J. and Rothenburg, L., Note on a random isotropic granular material with negative Poisson's ratio. *Int. J. Eng. Sci.*, 1988, **26**, 373–383.
9. Bathurst, R. J. and Rothenburg, L., Investigation of micromechanical features of idealized granular assemblies using DEM. Proceedings of the 1st US Conference on Discrete Element Methods, Golden, Colorado, 1989, p. 12.
10. Bathurst, R. J. and Rothenburg, L., Observations on stress-force-fabric relationships in idealized granular materials. *Mech. Mater.*, 1990, **9**, 65–80.
11. Rothenburg, L. and Bathurst, R. J., Analytical study of induced anisotropy in idealized granular materials. *Géotechnique*, 1989, **39**, 601–614.
12. Sitharam, T. G., Numerical simulation of hydraulic fracturing in granular media. PhD thesis, University of Waterloo, Waterloo, Ontario, 1991.
13. Thornton, C. and Barnes, D. J., Computer simulated deformation of compact granular assemblies. *Acta Mechanica*, 1986, **64**, 45–61.
14. Thornton, C., Computer simulated experiments on particulate materials. *Tribology in Powder Technology* (eds Briscoe, B. J. and Adams, M. J.), Adam Higher, Bristol, 1987, pp. 292–302.
15. Mirghasemi, A. A., Rothenburg, L. and Matyas, E. L., Influence of particle shape on engineering properties of two-dimensional polygon-shaped particles. *Géotechnique*, 2002, **52**, 209–217.
16. Cundall, P. A. and Strack, O. D. L., A discrete numerical model for granular assemblies. *Geotechnique*, 1979, **29**, 47–65.
17. Strack, O. D. L. and Cundall, P. A., Fundamental studies of fabric in granular materials. Interim Report to National Science Foundation, Department of Civil and Mineral Engineering, University of Minnesota, Minneapolis, Minnesota, 1984, p. 53.
18. Tang-Tat Ng, Numerical simulation of granular soil under monotonic and cyclic loading: A particulate mechanics approach. Ph D thesis, Rensselaer Polytechnic Institute, Troy, New York, 1989.
19. Chantawarungal, K., Numerical simulations of three dimensional granular assemblies. Ph D thesis, University of Waterloo, Waterloo, Ontario, 1993.
20. Itasca, Particle flow code in 3 dimensions. Software programme, 1999.
21. Thornton, C., Numerical simulations of deviatoric shear deformation of granular media. *Géotechnique*, 2000, **50**, 43–53.
22. Sitharam, T. G., Dinesh, S. V. and Shimizu, N., Phase transformation behaviour in granular materials using DEM. Proceedings of the Fourth International Conference on Micromechanics of Granular Media Powders and Grains 2001, Sendai, Japan, 2001, pp. 241–245.
23. Sitharam, T. G., Dinesh, S. V. and Shimizu, N., Micromechanical modelling of monotonic drained and undrained behaviour of granular media using three-dimensional DEM. *Int. J. Numer. Anal. Method Geomech.*, 2002, **26**, 1167–1189.
24. Dinesh, S. V., Discrete element simulation of static and cyclic behaviour of granular media. Ph D thesis, Indian Institute of Science, Bangalore, 2002.
25. McDowell, G. R. and Harireche, O., Discrete element modelling of soil particle fracture. *Géotechnique*, 2002, **52**, 131–135.
26. McDowell, G. R. and Harireche, O., Discrete element modelling of yielding and normal compression of sand. *Géotechnique*, 2002, **52**, 299–304.
27. Sitharam, T. G. and GovindaRaju, L., Evaluation of dynamic properties of sandy soils at large strain levels. Proceedings of the workshop on Current Practices and Future Trends in Earthquake Geotechnical Engineering, 23–24 December 2003, pp. 53–60.
28. Kokusho, K., Cyclic triaxial test of dynamic soil properties for wide strain range. *Soil. Found.*, 1980, **20**, 45–60.
29. Yasuda, N. and Matsumoto, N., Dynamic deformation characteristics of sands and rockfill materials. *Can. Geotech. J.*, 1993, **30**, 747–757.
30. Ishihara, K., Tatsuoka, K. and Yasuda, S., Undrained deformation and liquefaction of sand under cyclic stresses. *Soil. Found.*, 1975, **15**, 29–44.
31. Tatsuoka, F. and Ishihara, K., Drained deformation of sand under cyclic stresses reversing direction. *Soil. Found.*, 1974, **14**, 51–65.

ACKNOWLEDGEMENTS. We acknowledge the Department of Science and Technology (DST), Govt. of India, for the financial support for the project "In situ evaluation of soil liquefaction potential" under the grant No: DST/23/ (287)/SU/2001.